An Optimization Framework for Dynamic Hybrid Energy Systems

Wenbo Du[1] Humberto E. Garcia[1] Christiaan J.J. Paredis[2]

wenbo.du@inl.gov humberto.garcia@inl.gov chris.paredis@gatech.edu

[1]Idaho National Laboratory
750 University Boulevard, Idaho Falls, ID 83415-3570, USA

[2]Georgia Institute of Technology
813 Ferst Drive, Atlanta, GA 30332-0405, USA

Abstract

A computational framework for the efficient analysis and optimization of dynamic hybrid energy systems (HES) is developed. A microgrid energy system with multiple inputs and multiple outputs (MIMO) is modeled using the Modelica language in the Dymola environment. The optimization loop is implemented in MATLAB, with the FMI Toolbox serving as the interface between the computational platforms. Two characteristic optimization problems are selected to demonstrate the methodology and gain insight into the system performance. The first is an unconstrained optimization problem that optimizes intrinsic properties of the base generation, power cycle, and electrical storage components to minimize variability in the HES. The second problem takes operating and capital costs into consideration by imposing linear and nonlinear constraints on the design variables. Variability in electrical power applied to high temperature steam electrolysis is shown to be reduced by 18% in the unconstrained case and 11% in the constrained case. The preliminary optimization results obtained in this study provide an essential step towards the development of a comprehensive framework for designing HES.

Keywords: hybrid energy systems; dynamic simulation; optimization; renewable energy; FMI

1 Introduction

Hybrid energy systems (HES), which may combine multiple energy resources to achieve improved performance or cost efficiency, have attracted considerable attention in the United States and internationally due to developments in renewable energy technologies as well as economic, political, and environmental concerns regarding existing energy infrastructures. One notable challenge to the design and deployment of HES is the difficulty in modeling the operation and performance of such systems. Traditionally, electricity is produced from baseload generation (e.g., nuclear and coal plants), which operate at near steady state conditions with little variability. In contrast, renewable energy sources (e.g., wind turbines and concentrated solar plants) are highly dynamic with very significant variability. The addition of a renewable component to the energy infrastructure creates an enormous increase in the number of possible operational situations that must be considered, and thus greatly complicates the design process. Although it is well understood that a large energy storage device capable of achieving high rates of charge and discharge is necessary for mitigating the variability of renewable energy sources, the design and control of HES makes little use of proper design optimization methodology. In this study, we seek to apply optimization methods in order to gain a better understanding of the complex dynamics governing HES, and to obtain insights towards how to properly design such systems to maximize performance and cost efficiency.

To achieve the desired improvements in HES design, appropriate simulation and optimization tools need to be selected. The Modelica language is well suited for studying complex systems such as HES due to its object-oriented structure and acausal approach to modeling. On the other hand, the MATLAB environment provides a variety of optimization methods,

including those available in the Optimization Toolbox. In numerical optimization, it is of critical importance to automate the simulation process, because manual iterations quickly become impractical as the problem size is increased. Since our HES model and optimization algorithms are implemented in different software environments, a suitable tool for coupling diverse numerical tools is required. For this purpose, we use Functional Mockup Interface (FMI), which has been successfully demonstrated for both model exchange [1] and co-simulation [2]. In the present framework, we apply the FMI for model exchange.

The organization of the paper is as follows. First, we introduce the computational framework established in this study, with a brief summary of the HES model formulation and optimization approach. We then present two benchmark optimization problems to demonstrate the established methodology, followed by a discussion of the simulation and optimization results. Finally, we offer some concluding remarks in addition to an overview of future research directions related to this topic.

2 Computational framework

An illustration of the computational framework established in this paper is provided in Figure 1.

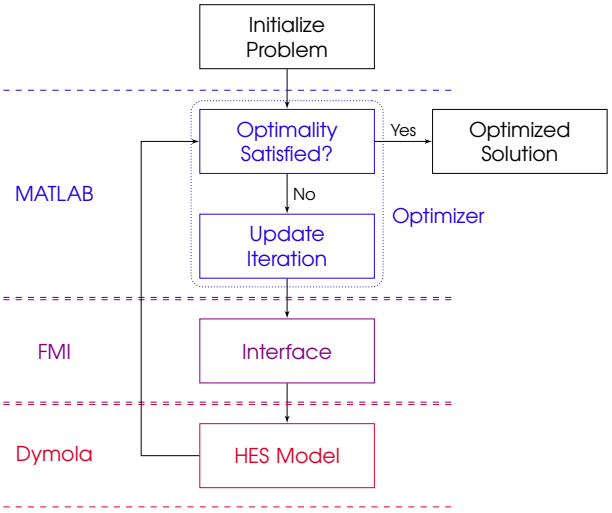

Figure 1: Schematic of computational framework.

Note that, as previously mentioned, the FMI is used to allow the MATLAB-based optimizer to modify inputs to the HES and setup additional simulations by building a Functional Mockup Unit (FMU) of the Modelica HES model. Also note that the optimization loop conducted in MATLAB may require a large number of iterations before converging to the optimized solution, and thus it is important that the HES model be sufficiently robust and flexible to handle a variety of potential operating scenarios. In the following section, we present the HES model considered in this work and discuss the concepts used in creating the model to ensure this robustness.

2.1 HES model

As mentioned above, the HES model considered in this work is implemented in the Dymola environment of the Modelica modeling language. As shown in Figure 2, the HES model has a configuration that includes multiple energy inputs and outputs. In this case, thermal and electrical energy in excess of the demand to the grid is dynamically distributed to a high temperature steam electrolysis (HTSE) process, which produces chemical products (hydrogen and oxygen) to complement the electricity produced by the HES. In a traditional hybrid energy system, multiple input energy sources are combined to provide a single output (MISO), i.e., electricity. The drawback of such a configuration is that in case the energy supply exceeds the demand, excess energy is either wasted or must be transferred to large storage devices, which are expensive. Therefore, the MIMO system can be expected to offer significant advantages in flexbility, utilization and efficiency over the MISO system, as reported in, for example, [3, 4].

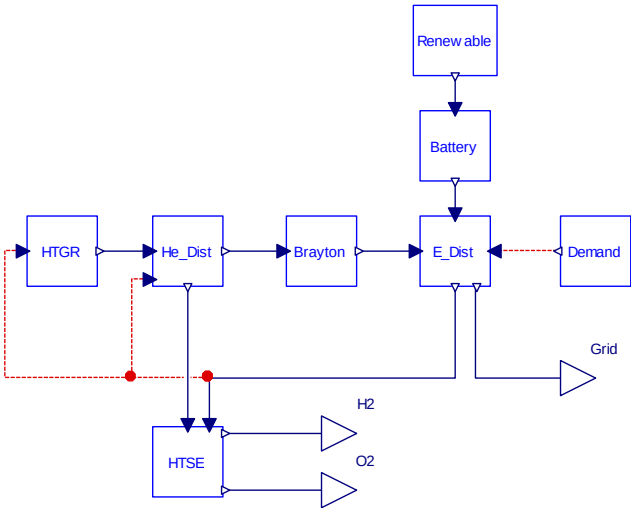

Figure 2: Model of Advanced HES configuration, implemented in Dymola.

Note that the HES considered here contains two types of energy flows: thermal (in the form of heated helium) and electrical. The conversion of thermal to

DOI 10.3384/ECP14096767

electrical energy occurs in the Brayton power plant, where heated helium (the working fluid) carries thermal energy provided by a high temperature gas reactor (HTGR). Electrical power from the Brayton plant is combined with that produced by a wind turbine (the renewable source), which is regulated by an electrical battery. Two distribution centers, one for helium and one for electricity, are used to dynamically calculate the amount of each energy type to be distributed to the HTSE to match the necessary electrical power output to the grid. Note that the HES model in Figure 2 includes two types of arrows: the solid (blue) arrows represent energy flows (helium and electricity), while the dotted (red) arrows represent information flows. For example, the amount of electricity distributed to the HTSE unit is needed at the HTGR and helium distribution center to calculate the required mass flow rate of helium. Similarly, the electricity distribution center makes use of information about the electricity demand in the grid to calculate the relative amount of electricity to be dynamically distributed between the grid and HTSE. For computational simplicity, detailed components within the subsystems such as pipes, valves, turbines, etc. are not considered in this initial effort; the system dynamics are instead captured by a series of transfer functions, switches, logic blocks, and other signal-based elements. The plan is to eventually replace these with models that more accurately capture the relevant physics; this topic is discussed further in the *Conclusions and future work* section. We next detail the models for the individual subsystems and components in the present computational framework.

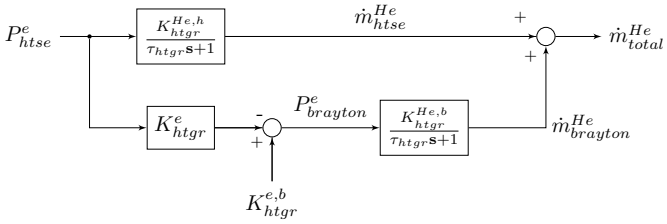

Figure 3: High temperature gas reactor model.

A schematic diagram for the HTGR is shown in Figure 3. The electrical power entering the HTSE (P^e_{htse}) is provided by the electricity distribution center, and is the input to the HTGR. The HTGR model then uses this information to calculate the amount of high temperature helium that would correspondingly be needed by the HTSE. Also note that the total amount of helium entering the Brayton plant is controlled by the amount of electricity directed to the HTSE. In an actual reactor, the operating conditions and output should ideally be constant, as fluctuations can cause excessive wear on the components and significantly shorten the lifespan of the system. Therefore, the variability in the HTGR generation will be an important component to the cost function used in the optimization of the HES in future work.

Revisiting Figure 2, we note that the mass of heated helium from the HTGR then enters the helium distribution center, where some of the helium is channeled to the HTSE for chemical production and the remainder is sent to the Brayton plant for electricity generation. As in the HTGR, the amount of electricity entering the HTSE is used as an input to the helium distribution center to calculate the flow of helium that needs to be directed to the HTSE to achieve near-stoichiometric conditions there. This is accomplished with the following equations:

$$\dot{m}^{He}_{brayton} = \dot{m}^{He}_{total} - \dot{m}^{He}_{htse} \tag{1}$$

$$\dot{m}^{He}_{htse} = K^{He}_{htse} P^e_{htse} \tag{2}$$

The Brayton plant is represented by a first-order transfer function

$$H_{brayton}(\mathbf{s}) = \frac{K^e_{brayton}}{\tau_{brayton}\mathbf{s}+1} \tag{3}$$

where the gain $K^e_{brayton}$ is a lumped quantity that accounts for efficiency and unit conversions, and the time constant $\tau_{brayton}$ can be varied according to the design and operation of the Brayton plant.

The Brayton power plant is one source of electricity in the system; the other is a series of wind turbines, which serve as the renewable source in this HES configuration. Note that as shown in Figure 2, the wind power is not inputted directly to the electricity distribution center, but via a grid-scale battery. This is because the battery model does not model the charge and discharge behavior of the battery directly, but rather the operational impact of the battery on dampening excessive unsteadiness due to high variability in available wind power. The renewable power is modeled as a time-varying input signal to the battery based on available wind speed data from the National Renewable Energy Laboratory (NREL), for a site in Wyoming.

As shown in Figure 3, there are four operating regimes for a wind turbine, separated by critical wind speed values. At wind speeds below a minimum cut-in velocity, there is insufficient kinetic energy in the wind to cause any rotation, and thus no electrical power is produced. At wind speeds above a cut-out velocity, a braking system is activated for safety reasons,

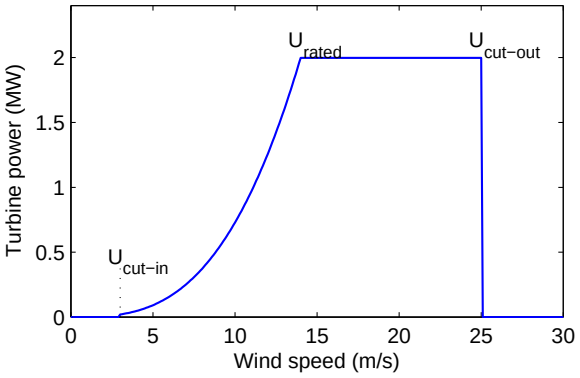

Figure 4: Turbine power vs wind speed.

and again no power is produced. Between the rated and the cut-out velocity values, the turbine provides a steady maximum power level, also known as the rated power. Finally, for the range between the cut-in and rated speeds, the power is calculated by the following equation:

$$P = \eta \frac{1}{2} \rho U^3 \frac{\pi d^2}{4} \tag{4}$$

where η is the conversion efficiency of the wind turbine, ρ is the density of the air at the site, U is the wind velocity, and d is the diameter of the turbine blades. In essence, this equation relates the power delivered by the turbine to the amount of kinetic energy available in the wind, via an overall lumped efficiency number. At a typical site, the majority of the turbine operation occurs in this regime.

Like the Brayton plant, the battery is modeled using a first-order transfer function:

$$H_{battery}(\mathbf{s}) = \frac{1}{\tau_{battery}\mathbf{s}+1} \tag{5}$$

We assume the maximum power delivered by the battery is equal to the renewable power, so a unity gain is used. It is important to not confuse the time constant $\tau_{battery}$ with the charge or discharge rate of the battery. Instead, the time constant is used to characterize the smoothing effect that the battery would have on the electricity delivered by a renewable and battery arrangement.

Electrical power from the Brayton plant $P^e_{brayton}$ and the renewable and battery arrangement $P^e_{battery}$ are combined in the electricity distribution center. The electrical distribution center contains a logic block that dynamically calculates the distribution of electricity to the grid and HTSE. When the combined electrical power P^e_{avail} is less than the grid demand, all available power is directed to the grid. When excess power is available, it is directed to the HTSE. This is modeled using the following equations:

$$P^e_{avail} = P^e_{brayton} + P^e_{battery} \tag{6}$$

$$P^e_{grid} = \begin{cases} P^e_{demand} & \text{if} \quad P^e_{avail} > P^e_{demand} \\ P^e_{avail} & \text{otherwise} \end{cases} \tag{7}$$

$$P^e_{htse} = \begin{cases} P^e_{avail} - P^e_{demand} & \text{if} \quad P^e_{avail} > P^e_{demand} \\ 0 & \text{otherwise} \end{cases} \tag{8}$$

Finally, electricity and helium energy flows are combined in the HTSE system, whose corresponding model is shown in Figure 5.

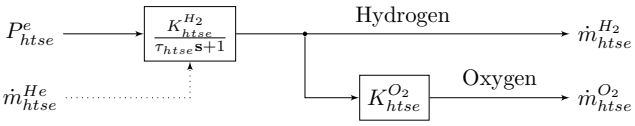

Figure 5: High temperature steam electrolysis model.

As illustrated by the dotted line in Figure 5, the mass flow rate of helium $\dot{m}^{He}_{htse}$ enters the HTSE but is not used in any calculations. This is because the helium distribution center ensures that the appropriate flow of helium is directed to the HTSE in accordance with the amount of electricity being consumed there. Therefore, only one of the two parameters is needed in the HTSE model.

Values of all simulation parameters, including gains in the blocks shown in Figures 3 and 5, can be found in Table 1 in section 3.

2.2 Optimization methodology

A general optimization problem can be written as a function minimization problem, as follows:

$$\text{minimize} \quad f(x), \quad f : \Re^n \to \Re \tag{9}$$

In general, the values of the design variables x are selected within a bounded range, while satisfying inequality constraints c_k and equality constraints $\hat{c}_j$:

$$\text{subject to} \quad \begin{cases} x_{lower} \leq x \leq x_{upper} \\ c_k(x) \leq 0, \quad k = 1,...,m \\ \hat{c}_j(x) = 0, \quad j = 1,...,\hat{m} \end{cases} \tag{10}$$

Solving this general optimization problem requires an algorithm that iteratively adjusts the values of the design variables until some termination criterion regarding the values of the objective and constraint functions is met, most commonly when the Karush-Kuhn-Tucker (KKT) conditions are satisfied [5]. Many different types of optimizers have been developed and applied to a wide variety of engineering problems. These

DOI 10.3384/ECP14096767

include gradient-based and gradient-free methods, as well as hybrid approaches for mixed-integer problems [6, 7] and surrogate-based methods [8, 9]. As shown in Figure 1, in this case we adopt a black-box optimization approach, in which the optimization algorithm uses the HES model output to update each iteration of the optimization loop, but does not access any state variables within the HES model. In selecting an appropriate optimization algorithm, it is important to consider the nature of the objective function and associated design variables, and match the optimizer according to the mathematical properties of the problem. In general, gradient-based methods converge more efficiently than gradient-free methods, and are thus preferred for smooth problems [10]. However, the objective function in this study, defined in section 3 as the total variability in the electrical power delivered to the HTSE, is very noisy with a large number of local minima that are problematic for gradient-based methods. Since the optimization routine is conducted in MATLAB, we select the *fminsearch* function as the optimizer. This is an implementation of the Nelder-Mead simplex method [11] included in the MATLAB Optimization Toolbox.

The Nelder-Mead method creates a simplex with $n+1$ vertices in an n-dimensional design space, and iteratively manipulates the size and shape of the simplex using operations such as reflection, expansion, contraction and reduction based on the relative objective function values at the vertices. The method is gradient-free because only the values of the objective functions at the vertices are used, and thus it is suitable for noisy or discontinuous functions. The general Nelder-Mead method is valid for unconstrained optimization problems; to handle constraints, we modify the objective function $f(x)$ by introducing a penalty function:

$$\hat{f}(x) = f(x) + p(x) \tag{11}$$

The penalty function $p(x)$ is equal to zero in the feasible space, and gives a positive value when a constraint is violated. We then apply the optimizer to minimize the modified objective function $\hat{f}(x)$ instead of the original function $f(x)$. We use a quadratic form of the penalty function that can be easily computed:

$$p(x) = \rho \sum_{i=1}^{m+\hat{m}} \max(0, c_i)^2 \tag{12}$$

where m and $\hat{m}$ are the number of inequality and equality constraints, respectively. This penalty function is valid for both inequality and equality constraints [12]. The coefficient ρ must be large enough to force the optimizer into the feasible space when a constraint is violated; a value of $\rho = 10$ is found to be sufficient in this study.

The time constants of the HTGR, Brayton plant, and battery are designated as the design variables. Although the Nelder-Mead simplex method has been shown to suffer from poor convergence rate for problems involving a large number of design variables, it is suitable for the three variables considered here [13].

3 Problem formulation

Available wind velocity data are sampled at time intervals of 600 seconds; we conduct our simulations with the same time step size in order to avoid numerical errors that would arise from interpolating between data points. All simulations are conducted for a time period of one week (6.048×10^5 seconds), for a total of 1009 time steps per simulation. This time period is selected to balance the need to capture the effects of variability in the renewable energy input, with the need to conduct simulations at a feasible computational cost. As shown in Figure 6, the wind turbine experiences very fast dynamics, with numerous transient peaks and valleys observed in the velocity and power profiles within a single week. This high degree of variability confirms that the time period selected provides a representative sample of the overall long-term variability in renewable energy input experienced by the HES.

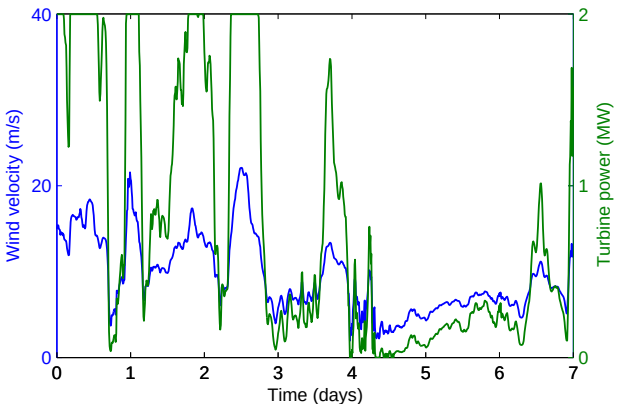

Figure 6: Wind velocity and turbine power profiles for one week sample time period.

Since the properties of the wind turbine are assumed to be constant throughout the simulations, we lump all of these values from Equation 4 together, such that each individual turbine provides maximum of 2 MW rated power. This is equivalent to an overall conversion efficiency of 55%, air density of 1.2 kg/m^3 and

	Parameter	Symbol	Value	Units
HTGR	Power output	$K^{e,b}_{htgr}$	135	MWe
	He reactor gain	$K^{He,h}_{htgr}$	0.464	kg/MJ
	Power to mass flow	$K^{He,b}_{htgr}$	1.06	kg/MJ
	Electrical gain	K^{e}_{htgr}	0.0838	-
Brayton	Mass flow to power	$K^{e}_{brayton}$	0.9429	MJ/kg
HTSE	H_2 gain	$K^{H_2}_{htse}$	0.00724	kg/MJ
	O_2 gain	$K^{O_2}_{htse}$	7.94	-
	Time constant	τ_{htse}	1	s
Wind	No. of turbines	n_T	15	-
	Cut-in speed	U_{cut-in}	3	m/s
	Rated power speed	U_{rated}	14	m/s
	Cut-out speed	$U_{cut-out}$	25	m/s
Grid	Target load	P_{demand}	100	MWe

Table 1: Fixed system properties and simulation parameters.

turbine diameter of 53 m, for an overall gain value of k_{wind} = 7.28×10^{-4} MW-s^3/m^3 between the cut-in and rated power wind speeds:

$$P = k_{wind} U^3 \tag{13}$$

We also simplify the scaling problem by assuming that the individual turbines, which constitute the renewable component of the HES, are separated sufficiently far apart so as to not experience mutual interference. A simple linear scaling in renewable power with the number of turbines is thus used.

The fixed simulation parameter values are listed in Table 1. The thermal and electrical outputs from all system components are initialized to be zero in order to analyze the impact of the initial start-up phase on the overall system performance, and a constant electricity profile of 100 MWe delivered from the HES to the grid is assumed. For simplicity, we select a fixed HTGR power output (135 MWe) that exceeds this output level to ensure that the HTSE unit can be operated continuously even when no renewable power is provided to the system. This is necessary because frequently shutting down the HTSE process entails a high cost while also making the system susceptible to damage.

Given these considerations, it is logical to design HES in which energy flow variability is minimized. For this purpose, we define the objective function to be minimized in our optimization problem as the total amount of variability in the electrical power input to the HTSE:

$$P^e_{var}(t) = |P^e_{htse}(t) - \bar{P}^e_{htse}| \tag{14}$$

$$f(x) = \int_0^{t_f} P^e_{var}(t)dt \tag{15}$$

where the quantity $\bar{P}^e_{htse}$ is the time-averaged value of electrical power input to the HTSE.

For optimization, this integral can be approximated by first computing $\bar{P}^e_{htse}$, and then applying a numerical integration scheme to the HES simulation data. Using the trapezoidal method, we obtain the following form of the objective function used by the optimizer:

$$f(x) = \sum_{i=1}^{n} (t_i - t_{i-1}) \frac{P^e_{var,i} + P^e_{var,i-1}}{2} \tag{16}$$

where n = 1009 is the number of time steps.

We consider two optimization problems, one unconstrained and one constrained. Three design variables are considered in both cases: the time constants for the battery ($\tau_{battery}$), HTGR (τ_{htgr}), and Brayton cycle ($\tau_{brayton}$). In the unconstrained case, the design variables are bounded but allowed to vary independently. An arbitrary baseline case ($\tau_{battery}$ = 3600 s, τ_{htgr} = 1200 s, $\tau_{brayton}$ = 600 s) is used as the starting point for the optimization routine, and the following upper and lower bounds shown in Table 2 are specified.

Variable	Minimum	Maximum
$\tau_{battery}$ (s)	1800	18000
τ_{htgr} (s)	240	3600
$\tau_{brayton}$ (s)	180	3600

Table 2: Upper and lower bounds on design variables.

From an understanding of the physics governing the performance of the system, we can expect the optimizer to converge towards these bounds in the absence of constraints. This is because a larger time constant for the battery allows greater smoothing of the variability in the wind power profile, thus reducing the variability of electricity distributed to the HTSE. Conversely, a smaller time constant for the HTGR and power cycle allows them to track the electrical power demanded by the grid more closely, which again would reduce variability in electricity directed to the HTSE. Due to this understanding of the expected solution, the unconstrained optimization problem serves as a good benchmark case to verify whether the optimizer performs as expected.

Of course, the unconstrained case provides limited insight into the design of HES, because there are important constraints that need to be considered. As the time constant of the battery increases, so does the minimum battery size required to accommodate the necessary charging and discharging. This is illustrated in Figure 7, where the renewable power profiles, with and without the operation of the battery, are plotted together for three different battery time constants. To

DOI 10.3384/ECP14096767

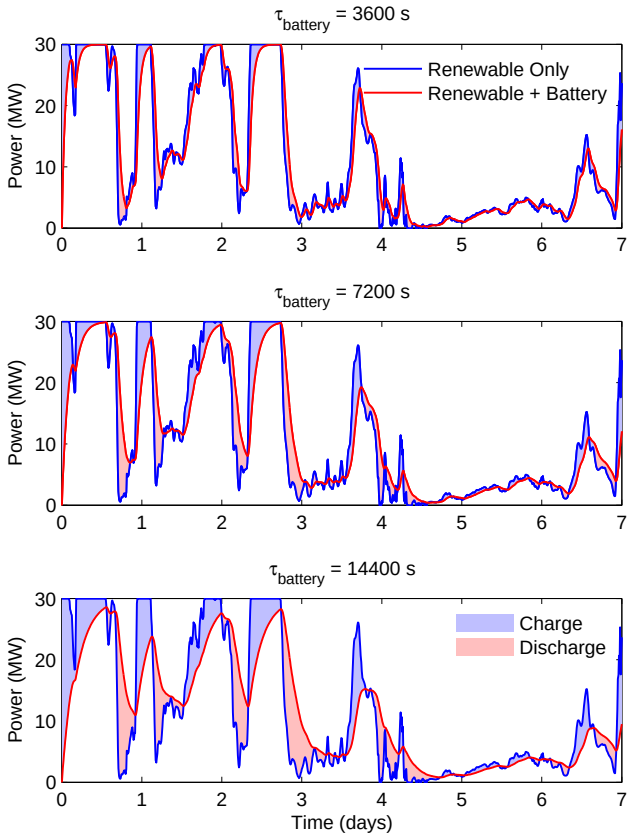

Figure 7: Effect of time constant on required battery size and delivered electrical power.

facilitate a comparison between the three cases, the difference between the two profiles is shaded (blue for when the battery is being charged, red for when it is being discharged). The required battery size (in terms of energy storage capacity) is represented by the largest shaded area, and is observed to increase with the battery time constant. Since the capital and operating costs of the battery are directly related to its size, it is clear that a constraint is needed to assess a penalty to increasing its time constant. Similarly, the time constant for the HTGR and Brayton plant cannot be arbitrarily decreased, as faster dynamics put a greater strain on the system components and lead to damage and reduced reliability - ultimately leading to increased total cost.

To address these cost issues, we consider a second optimization problem in which the following linear constraint is applied to the design variables:

$$c_1(x) = k_1\tau_{battery} - k_2\tau_{htgr} - k_3\tau_{brayton} - k_4 \leq 0 \quad (17)$$

where the weighting coefficients (k_1=1, k_2=3.5, k_3=1) reflect the relative cost associated with each component. The nuclear reactor is the most capital-intensive of the three, and thus has the highest weight applied to it in the constraint function. Note that the signs of the coefficients manipulate the optimizer into decreasing $\tau_{battery}$ while increasing τ_{htgr} and $\tau_{brayton}$. The coefficients are selected such that the constant term vanishes ($k_4 = 0$).

In addition to the linear constraint in Equation 17, we also apply two nonlinear constraints governing the relative speeds of the HTGR and Brayton cycle:

$$c_2(x) = \frac{\tau_{htgr}}{\tau_{brayton}} - 2 \leq 0 \quad (18)$$

$$c_3(x) = \frac{\tau_{brayton}}{\tau_{htgr}} - 2 \leq 0 \quad (19)$$

These two constraints are included to ensure that neither component becomes a significant bottleneck to the other. Note that all constraints in this case are inequality constraints; our optimization problem does not consider equality constraints (i.e., $\hat{c}_j(x)$ in Equation 10).

4 Results and discussion

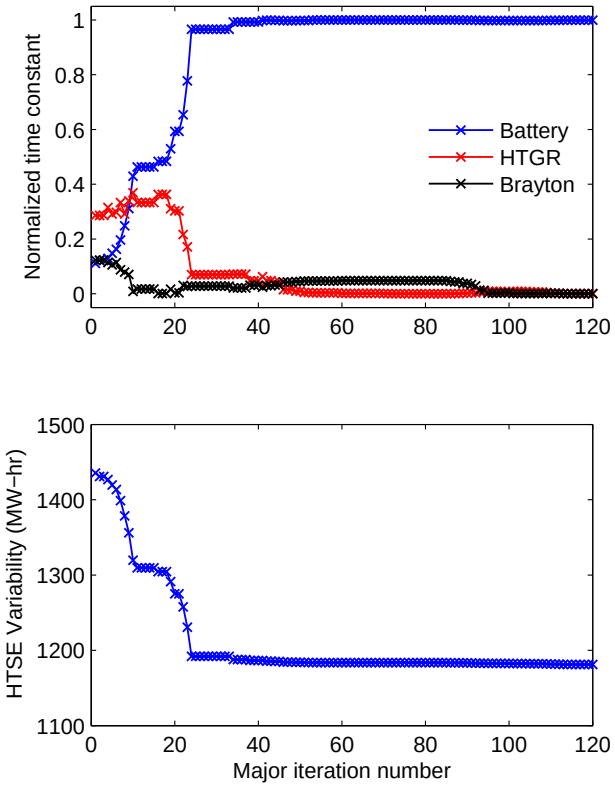

Figure 8: Progression of design variables (top) and objective function (bottom) for unconstrained optimization problem.

Optimization results for the unconstrained problem are shown in Figure 8. For illustration purposes, non-dimensional time constants are plotted by normalizing

using the upper and lower bounds reported in Table 2:

$$\tau_i^* = \frac{\tau_i - \tau_{i,\min}}{\tau_{i,\max} - \tau_{i,\min}} \tag{20}$$

As expected, the optimizer converges the battery time constant to the upper bound, and the others to their lower bounds. The value of the objective function at the optimum is $f(x)$ = 1181.1 MW-hr, which represents a reduction of 17.7% in the HTSE electrical power variability. Although this may not seem like an especially large improvement, the impact can in fact be quite substantial due to the highly capital-intensive nature of HES. A substitution of the unconstrained optimum into Equation 17 shows that the linear cost constraint is not satisfied, and thus the unconstrained optimum is not a feasible solution for the constrained problem.

As shown in Figure 9, the constrained optimum is located at $\tau_{battery}$ = 15311 s, τ_{htgr} = 3600 s, $\tau_{brayton}$ = 2712 s, with HTSE variability of $f(x)$ = 1275.5 MW-hr - a 11.2% improvement over the baseline case. The HTGR time constant experiences the most significant change compared to the unconstrained case, increasing from its minimum to its maximum bound. This is due to the high weighting assigned to the cost constraint c_1. Although the HTSE variability is increased by 6.5% compared to the unconstrained case, this loss is outweighed by the benefits in operational costs due to fast reactor dynamics. Note that in the final solution, the linear constraint c_1 is active since the constraint function value is equal to numerical zero, while the nonlinear constraints c_2 and c_3 are inactive. This can be verified by inspection using Equations 17-19. A comparison of the optimization solutions with respect to the baseline case is summarized in Table 3.

	Baseline	Unconstrained	Constrained
$\tau_{battery}$ (s)	3600	18000	15311
τ_{htgr} (s)	1200	240	3600
$\tau_{brayton}$ (s)	600	180	2712
$f(x)$ (MW-hr)	1435.4	1181.1	1275.1

Table 3: Design variables and objective function results for baseline, unconstrained, and constrained cases.

In addition to considering the values of the design variables, constraints and objective function at the optima, it is also important to examine the HES simulations themselves to gain a better understanding of the physics occurring within the system. Figure 10 plots the electrical power profiles in the HTSE for the three cases, as well as the mean power level in each case.

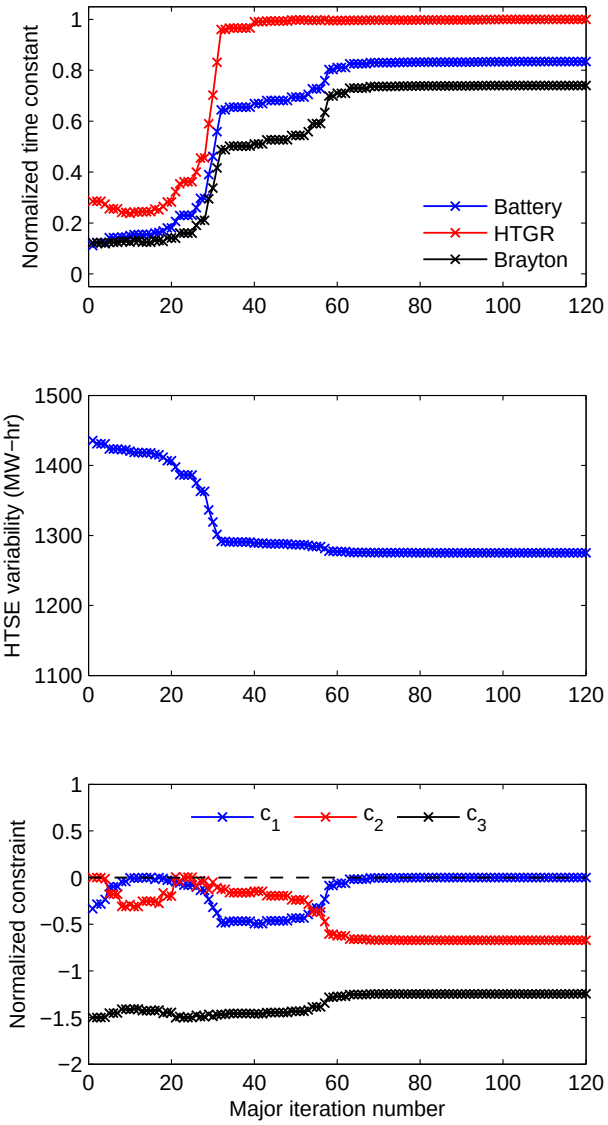

Figure 9: Progression of design variables (top), objective function (middle), and constraints (bottom) for constrained optimization problem.

The shaded area between the two is the numerically integrated area used to compute the value of the objective function. We note that in both optimization cases, not only is the total shaded area reduced, but the power profile is also generally smoother, with fluctuations of lesser amplitude and frequency. The main difference between the unconstrained and constrained solutions occurs in the initial ramping of the HTSE, where the constrained case incurs a substantial penalty due to slower reactor and power cycle dynamics. This is a direct consequence of the initial conditions in the problem formulation. For example, a long-term analysis that ignores the start-up phase of the system would likely exhibit a smaller difference between the two solutions.

DOI 10.3384/ECP14096767

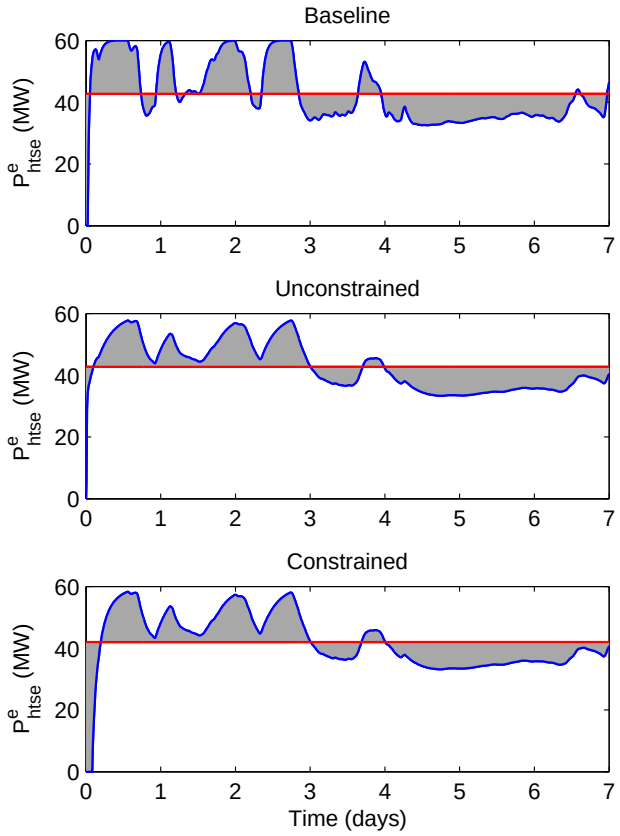

Figure 10: HTSE power profile for baseline, unconstrained, and constrained cases.

5 Conclusions and future work

In this paper, we have successfully established a computational framework for simulating and optimizing the performance of HES by interfacing the Modelica system model with analysis and optimization tools via the FMI for model exchange. Results from two optimization problems, one unconstrained and one constrained, illustrate the complex interplay between HES system components in the presence of high variability in the renewable power source. These preliminary results also highlight the difficulty of designing resilient and robust systems, again due to the high degree of variability and uncertainty over the lifespan of the system. The results obtained in this study represents an important step towards our goal of developing a flexible, efficient, and expandable framework for optimizing HES and achieving a level of understanding of the system dynamics and performance that would enable the deployment of HES in real world applications.

An important focus of future research efforts will be the models of the HES components. Since the main objective of the present study is to demonstrate the framework and to gain a better understanding of the performance of HES through simulations, the simplistic but computationally efficient signal-based HES model is considered adequate in this case. However, to properly utilize the available analysis and optimization tools, a system that more closely models the relevant physical phenomena is needed. This would entail replacing the signal block component models with, for example, process models for the HTSE [14] and equivalent-circuit models for the battery [15]. To retain reasonable computational cost, reduced-order models constructed using surrogate-based techniques may also be applied [16, 17, 18]. Furthermore, a comprehensive design process for such systems must take into account a large number of variables and constraints, which cannot be investigated to a sufficient level of detail using the present model. Therefore, current efforts are aimed at creating higher fidelity, physics-based models to incorporate into the computational framework established in this study.

Another topic that warrants future investigation is the comparison of different HES configurations and assessment of new technologies. A valuable benefit of conducting the simulations in Modelica is the flexibility of the resulting framework, allowing for certain model components to be readily replaced with those representing different technologies - and for the performance of the different systems to be directly compared. For instance, we may be interested in examining the relative performance of nuclear and natural gas power plants, or the relative cost of electrical versus thermal storage in grid-scale applications.

Finally, our present efforts have focused on design optimization - i.e., optimizing certain properties of the system components. Another equally important consideration, however, is the operation of the HES after it has been properly designed. In the present study, parameters related to the system operation (such as those located in the helium and electricity distribution centers) are assigned fixed empirical values; the proper operation of the system will require incorporation of additional factors such as economics and energy efficiency into optimization problems of much greater scale.

6 Acknowledgment

The present research efforts have been supported by the Energy Security Initiative (ESI) at Idaho National Laboratory (INL) under the United States Department of Energy contract DE-AC07-05ID14517.

References

[1] T. Blochwitz, M. Otter, M. Arnold, et al. The functional mockup interface for tool independent exchange of simulation models. In *Modelica'2011 Conference, March*, pages 20–22, 2011.

[2] M. Wetter. Co-simulation of building energy and control systems with the building controls virtual test bed. *Journal of Building Performance Simulation*, 4(3):185–203, 2011.

[3] H.E. Garcia, A. Mohanty, W.C. Lin, and R.S. Cherry. Dynamic analysis of hybrid energy systems under flexible operation and variable renewable generation–part i: Dynamic performance analysis. *Energy*, 52:1–16, 2013.

[4] H.E. Garcia, A. Mohanty, W.C. Lin, and R.S. Cherry. Dynamic analysis of hybrid energy systems under flexible operation and variable renewable generation–part ii: Dynamic cost analysis. *Energy*, 52:17–26, 2013.

[5] H.W. Kuhn and A.W. Tucker. Nonlinear programming. In *Proceedings of the second Berkeley symposium on mathematical statistics and probability*, volume 5. California, 1951.

[6] T. Victoire and A.E. Jeyakumar. Hybrid pso–sqp for economic dispatch with valve-point effect. *Electric Power Systems Research*, 71(1):51–59, 2004.

[7] N. Xue, W. Du, T.A. Greszler, W. Shyy, and J.R.R.A. Martins. Design of a lithium-ion battery pack for phev using a hybrid optimization method. *Applied Energy*, 158:591–602, 2014.

[8] R.A. Moore, D.A. Romero, and C.J.J. Paredis. A rational design approach to gaussian process modeling for variable fidelity models. In *Proceedings of ASME International Design Engineering Technical Conferences*, 2011.

[9] W. Du, N. Xue, A. Gupta, A.M. Sastry, J.R.R.A. Martins, and W. Shyy. Optimization of limn2o4 electrode properties in a gradient-and surrogate-based framework. *Acta Mechanica Sinica*, 29(3):335–347, 2013.

[10] N. Xue, W. Du, A. Gupta, W. Shyy, A.M. Sastry, and J.R.R.A. Martins. Optimization of a single lithium-ion battery cell with a gradient-based algorithm. *Journal of The Electrochemical Society*, 160(8):A1071–A1078, 2013.

[11] J.A. Nelder and R. Mead. A simplex method for function minimization. *The computer journal*, 7(4):308–313, 1965.

[12] J. Nocedal and S.J. Wright. *Penalty and Augmented Lagrangian Methods*. Springer, 2006.

[13] J.C. Lagarias, J.A. Reeds, M.H. Wright, and P.E. Wright. Convergence properties of the nelder–mead simplex method in low dimensions. *SIAM Journal on Optimization*, 9(1):112–147, 1998.

[14] J.E. O'Brien, M.G. McKellar, E.A. Harvego, and C.M. Stoots. High-temperature electrolysis for large-scale hydrogen and syngas production from nuclear energy–summary of system simulation and economic analyses. *International journal of hydrogen energy*, 35(10):4808–4819, 2010.

[15] X. Hu, S. Li, and H. Peng. A comparative study of equivalent circuit models for li-ion batteries. *Journal of Power Sources*, 198:359–367, 2012.

[16] W. Du, A. Gupta, X. Zhang, A.M. Sastry, and W. Shyy. Effect of cycling rate, particle size and transport properties on lithium-ion cathode performance. *International Journal of Heat and Mass Transfer*, 53(17):3552–3561, 2010.

[17] A. Gupta, J.H. Seo, X. Zhang, W. Du, A.M. Sastry, and W. Shyy. Effective transport properties of limn2o4 electrode via particle-scale modeling. *Journal of The Electrochemical Society*, 158(5):A487–A497, 2011.

[18] W. Du, N. Xue, A.M. Sastry, J.R.R.A. Martins, and W. Shyy. Energy density comparison of li-ion cathode materials using dimensional analysis. *Journal of The Electrochemical Society*, 160(8):A1187–A1193, 2013.

DOI 10.3384/ECP14096767